PROCEEDINGS OF THE ROYAL SOCIETY A

Proc. R. Soc. A (2012) **468**, 310–322
doi:10.1098/rspa.2011.0305
Published online 31 August 2011

Topology-dominated dynamic wetting of the precursor chain in a hydrophilic interior corner

By Quanzi Yuan and Ya-Pu Zhao*

State Key Laboratory of Nonlinear Mechanics, Institute of Mechanics, Chinese Academy of Sciences, Beijing 100190, People's Republic of China

The topology-dominated dynamic wetting of a droplet in a hydrophilic interior corner was explored using molecular dynamics simulations and molecular kinetic theory. A wetting transition in the interior corner of a single-file water-molecule precursor chain (PC), which eliminated the stress singularity and advanced much faster than the precursor film, was controlled by the interior angle. Owing to the confinement in the interior corner, the potential surface is lower and smoother. The one-dimensional hydrogen-bond chain transferred the disjoining pressure to drive the PC to slip-like ice. As an example, a stable and long metallic monatomic chain was formed using the unique transport properties of the PC for the first time. Our results may help in understanding the topology-dominated dynamic wetting in a hydrophilic interior corner, expand 'Taylor conjecture' to nanoscale and develop new applications at nanoscale.

Keywords: wetting; interior corner; precursor chain; molecular dynamics; molecular kinetic theory

1. Introduction

The dynamic wetting properties of topologically structured surfaces are great concerns of both science (Rascón & Parry 2000; Herminghaus *et al.* 2008; Bonn *et al.* 2009) and applications (Gleiche *et al.* 2000; Kwon *et al.* 2009; Patra *et al.* 2009). When placed on a hydrophilic surface, a droplet is driven by the surface tension to spread until its dynamic contact angle reaches an equilibrium value θ_0, known as the Young equation (Young 1805). If the droplet is placed in a hydrophilic interior corner with interior angle 2α, what will happen when the two contact lines of the droplet on wedge surfaces encounter at the corner? This conjecture can be traced back to Taylor (1712). Fastening two pieces of glass together, he found that the water would automatically rise in the hydrophilic interior corner with opening angle of 2.5°. Taylor conjectured the upper surface of the water in the interior corner to be hyperbola.

Then, in 1969 the Concus–Finn condition was mathematically introduced (Concus & Finn 1969): (i) for $\theta_0 > \pi/2 - \alpha$, the droplet wets in part the interior corner; (ii) for $\theta_0 < \pi/2 - \alpha$, the droplet completely wets the interior corner. Using

*Author for correspondence (yzhao@imech.ac.cn).

Electronic supplementary material is available at http://dx.doi.org/10.1098/rspa.2011.0305 or via http://rspa.royalsocietypublishing.org.

Received 16 May 2011
Accepted 1 August 2011

hydrodynamics, an exact solution for the spreading drop in an interior corner along with experimental verification was obtained (Weislogel & Lichter 1996). The topological structure of the interior corner leads to significant changes in the dynamic wetting properties (Weislogel & Lichter 1998; Chen *et al.* 2006).

The stress singularity in continuum theory is the seed for a new micro/nano structure. Owing to the no-slip boundary condition, Huh & Scriven (1971) pointed out that there would be a stress singularity at the moving contact line when a droplet spreads, and hence 'not even Herakles could sink a solid'. When viewed at the atomic level, a very thin precursor film (PF), usually a single molecular layer propagating ahead of the nominal contact line, is a crucial part in the dynamic wetting process (De Gennes 1985; Wang *et al.* 2009). PFs, which could eliminate the contact line singularity, are one of the answers to the Huh–Scriven paradox (Huh & Scriven 1971). Both experiments (Kavehpour *et al.* 2003) and simulations (mesoscopic: hydrokinetic lattice Boltzmann (LB) method (Chibbaro *et al.* 2008) and nanoscopic: molecular dynamics (MD) simulations (Webb *et al.* 2003) confirm the existence of PFs. In a hydrophilic interior corner, there is also a stress singularity adopting the continuum approach (Weislogel & Lichter 1998). And what happens if the two PFs meet with high speed at the interior corner ahead of the nominal contact line?

Liquid transport in the interior corner is a crucial requirement in a variety of application fields, such as aerospace (Wang *et al.* 2010), micro/nanofluidics (Khare *et al.* 2007), biology (Seemann *et al.* 2005), fuel cell (Spernjak *et al.* 2007), etc. It is of great interest to improve the transport velocity and work efficiency in these application fields. In addition, metallic monatomic chains (MACs) have received considerable attention for their ultimate miniaturization and novel functionality in electron transport properties in the last decade (Ohnishi *et al.* 1998; Tang *et al.* 2010). But, the formation of a stable and long MAC is still a challenging problem for nano-machining. Moreover, the enhanced flow in nanotubes is well known for its outstanding transport properties (Whitby & Quirke 2007). Is there a candidate in nanofluidics other than the enhanced flow in nanotube?

The answer to the earlier-mentioned theoretical puzzles and the application problems may be a new molecular structure: the precursor chain (PC).

We first employed MD simulations to explore the atomic details of a water droplet in a hydrophilic gold interior corner with different interior angles in dynamic wetting. Our results showed that the wetting transition is governed by the interior angle 2α. In the case of $2\alpha < 135°$, a PC completely wetted the interior corner; in the case of $2\alpha \geq 135°$, no apparent PC was observed; and the PF wetted in part the interior corner. The existence of the PC imports atomic details to eliminate the stress singularity in the interior corner. Then, molecular kinetic theory (MKT) was adopted to investigate the transport properties of the PC and found that: (i) the PC was driven by the disjoining pressure, whose energy could be obtained from theoretical derivations and MD results; (ii) because water molecules were confined in the interior corner, the potential surface near the interior corner is lower and smoother when compared with that on the bare surface, and quickly decayed in a distance of about a water molecule. Hence, the PC could generate, exist stably and propagate fast. In the PC, a one-dimensional hydrogen-bond (H-bond) chain transferred pressure to drive the PC to slip-like ice. With an increase in 2α, the potential surface near the interior corner became high and rough. The transport properties of the PC gradually tended to be the

same as those of the PF. In order to show the important role and applications of the PC as an example, for the first time, we used the unique transport properties of the PC to generate a MAC, which has received considerable attention for its ultimate miniaturization and novel functionality in electron transport properties in the last decade (Ohnishi *et al.* 1998; Tang *et al.* 2010). Our results may help in understanding the topology-dominated dynamic wetting, expanding 'Taylor conjecture' to nanoscale and developing new applications at nanoscale.

2. Computational methods

MD simulations implemented in a large-scale atomic/molecular massively parallel simulator (LAMMPS) (Plimpton 1995) were carried out under a constant temperature of 300 K for 0.1 μs to explore the transport properties of the PC in a gold interior corner. The simulation domain is shown in figure 1*a*,*b*. The interior angle 2α varied from 26.6°, 45°, 63.4°, 90°, 116.6° to 135°.

The extended simple point charge (SPC/E) water model (Berendsen *et al.* 1987) was used. The SPC/E model is a slight reparametrization of the simple point charge (SPC) model, with a modified value of q_{O} (charge on oxygen atoms) and q_{H} (charge on hydrogen atoms), in order to add an average polarization correction to the potential energy function. Both the oxygen atoms and hydrogen atoms in the SPC/E model were modelled as charged Lennard–Jones (LJ) particles with $\sigma_{\mathrm{O-O}} = 0.3166\,\mathrm{nm}$, $\varepsilon_{\mathrm{O-O}} = 0.650\,\mathrm{kJ\,mol^{-1}}$, $q_{\mathrm{O}} = -0.8476\,\mathrm{e}$ for oxygen atoms and $\sigma_{\mathrm{H-H}} = 0.0\,\mathrm{nm}$, $\varepsilon_{\mathrm{H-H}} = 0.0\,\mathrm{kJ\,mol^{-1}}$, $q_{\mathrm{H}} = 0.4238\,\mathrm{e}$ for hydrogen atoms. Compared with SPC, transferable intermolecular potential 3 point (TIP3P) and transferable intermolecular potential 4 point (TIP4P) models, the SPC/E model can obtain a better diffusion coefficient (Mark & Nilsson 2001), surface tension (Vega & De Miguel 2007) and viscosity (González & Abascal 2010), which control the spreading process, but without increasing the computational cost.

The gold atoms were modelled as uncharged LJ particles with $\sigma_{\mathrm{Au-Au}} = 0.2637\,\mathrm{nm}$, $\varepsilon_{\mathrm{Au-Au}} = 42.5723\,\mathrm{kJ\,mol^{-1}}$ and $q_{\mathrm{Au}} = 0.0\,\mathrm{e}$. The values of σ and ε between them were calculated according to the Lorentz–Berthelot rule: $\sigma_{\mathrm{X-Y}} = (\sigma_{\mathrm{X-X}} + \sigma_{\mathrm{Y-Y}})/2$ and $\varepsilon_{\mathrm{X-Y}} = (\varepsilon_{\mathrm{X-X}} \times \varepsilon_{\mathrm{Y-Y}})^{1/2}$, where X and Y represent the types of atoms. So $\sigma_{\mathrm{O-H}} = 0.1583$, $\sigma_{\mathrm{Au-H}} = 0.1319$, $\sigma_{\mathrm{Au-O}} = 0.2902\,\mathrm{nm}$ and $\varepsilon_{\mathrm{O-H}} = 0.0$, $\varepsilon_{\mathrm{Au-H}} = 0.0$, $\varepsilon_{\mathrm{Au-O}} = 5.2604\,\mathrm{kJ\,mol^{-1}}$. The total potential energy E_{ij} between two atoms i and j separated by r_{ij} is the sum of LJ potential energy and Coulombic pairwise interaction

$$E_{ij} = 4\varepsilon_{\mathrm{X-Y}}\left[\left(\frac{\sigma_{\mathrm{X-Y}}}{r_{ij}}\right)^{12} - \left(\frac{\sigma_{\mathrm{X-Y}}}{r_{ij}}\right)^{6}\right] + k_e\frac{q_{\mathrm{X}}q_{\mathrm{Y}}}{r_{ij}}, \tag{2.1}$$

where ε is the depth of the potential well, σ is the zero-crossing distance for the potential, $k_{\mathrm{e}} = 8.988 \times 10^9\,\mathrm{N\,m^2\,C^{-2}}$ is the Coulomb constant and q is the charge on the atom. The cut-off length for both LJ potential and Coulombic interaction is 1 nm.

The NVT ensemble (constant number of atoms, volume and temperature) was used. The Nosé–Hoover thermostat with a time-step of 1 fs was employed to regulate the temperature at 300 K. We specified a H-bond between water

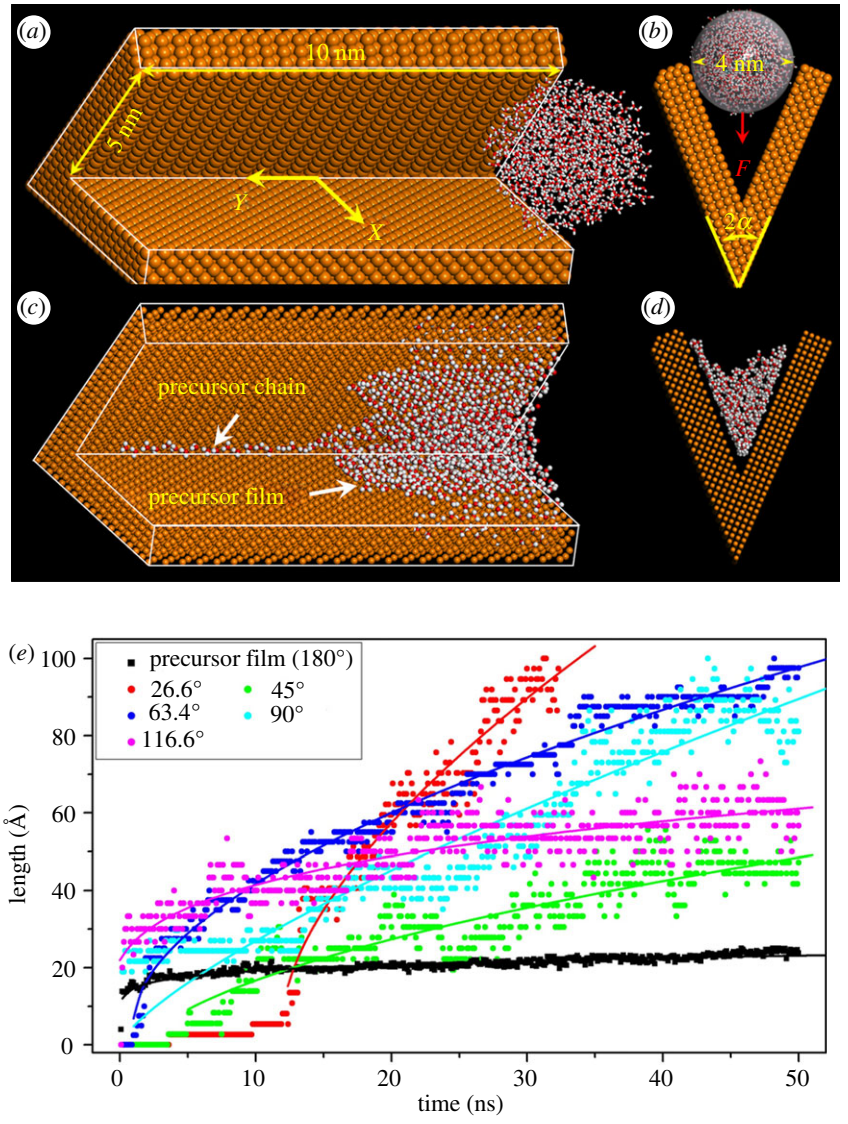

Figure 1. (*a*) Oblique view. (*b*) Cross section of the simulation domain. (*c*) Oblique view. (*d*) Cross section of the simulation result. The orange, red and white balls represent gold, oxygen and hydrogen atoms, respectively. (*e*) The propagation length of the PC with respect to the time (points: the molecular dynamics simulations; lines: the fit lines obeying the power law). The PC: red (26.6°), green (45°), blue (63.4°), cyan (90°) and purple (116.6°). The PF: black. The X and Y coordinates, which correspond to those in figures 3 and 4, locate on gold [100] surface. (Online version in colour.)

molecules if the O−O distance was less than 3.5 Å, and simultaneously, the angle O−H…O was greater than 100°.

The droplet was pulled along the bisector of the interior angle towards the interior corner by the attractive van der Waals (vdW) force F. Then, the droplet spreads on the substrate driven by the disjoining pressure. According

to the MD results, the wetting transition is controlled by the interior angle. In the case of $2\alpha < 135°$, an apparent PC advanced along the interior corner, whereas the PF advanced on the wedge surface, as shown in figure 1*c*,*d* for $2\alpha = 45°$. Obviously, the PC propagated much faster than the PF and completely wetted the interior corner. In the case of $2\alpha \geq 135°$, only the PF was observed and it wetted in part the interior corner, whereas no apparent PC could be found (see electronic supplementary material). The propagation length of the PC with respect to the time for different interior angle was plotted in figure 1*e*, which was fitted by the power law, similar to the treatment of the PF in the literature (Yuan & Zhao 2010). The velocity of PC v_{PC}, the slope of the length–time curve, is about $10^{-1}\,\mathrm{ms}^{-1}$, which is one order of magnitude higher than $v_{\mathrm{PF}} \sim 10^{-2}\,\mathrm{ms}^{-1}$. When 2α is small ($2\alpha = 26.6°, 45°$), the propagation length initially remained zero for a characteristic time of about 10 ns, during which the droplet was pulled to the interior corner.

Employing both mesoscopic LB and atomscopic MD methods, Chibbaro *et al.* (2008) simulate the capillary filling of highly wetting fluids in nanochannels and provide clear evidence of the formation of the PF, which obeys a square-root scaling law. In our simulations, the propagation of the PF and PC is confined by the finite volume of the droplet and driven by the disjoining pressure; so the PF advanced slower compared with Chibbaro *et al.*'s work and the PC's velocity decreased with an increase in the interior angle.

3. Results and discussion

How could the PC exist stably? Why could the PC propagate fast? To answer these questions, we adopt Eyring's MKT (Gladstone *et al.* 1941), to explain the mechanism behind these phenomena. The surfaces sites are separated by a distance λ ($\lambda = 4.08\,\text{Å}$ for gold [100] surface). When the water molecules jump between surface sites with potential well of H in height, the equilibrium frequency $\kappa_0 = (k_{\mathrm{B}}T/h)\exp(-H/k_{\mathrm{B}}T)$, where k_{B} and h are the Boltzmann and the Planck constant, respectively. When the water molecules are driven by the external driving work per unit area w, the advancing velocity of the water molecule

$$v = 2\kappa_0\lambda \sin\mathrm{h}\left(\frac{w}{2nk_{\mathrm{B}}T}\right) = 2\lambda\left(\frac{k_{\mathrm{B}}T}{h}\right)\exp\left(\frac{-H}{k_{\mathrm{B}}T}\right)\sinh\left(\frac{w}{2nk_{\mathrm{B}}T}\right) \tag{3.1}$$

where n is the number density of sites on the surface ($n = \lambda^{-2}$). In equation (3.1), w and H are variables and can be obtained from theoretical derivations or MD results; the others are all constants.

In our cases, w arises from the attractive vdW forces between the substrate and water molecules, namely the disjoining pressure (Derjaguin *et al.* 1987) and could be estimated theoretically. According to Philip's theoretical work (Philip 1977), using the polar coordinates (r, θ) as shown in figure 2*a*, the pressure P in the interior corner is

$$P(r,\theta) = \frac{A_{\mathrm{Au-Water}}}{48\pi}r^{-3}\left(3\cot\frac{\alpha+\theta}{2} + 3\cot\frac{\alpha-\theta}{2} + \cot^3\frac{\alpha+\theta}{2} + \cot^3\frac{\alpha-\theta}{2}\right) \tag{3.2}$$

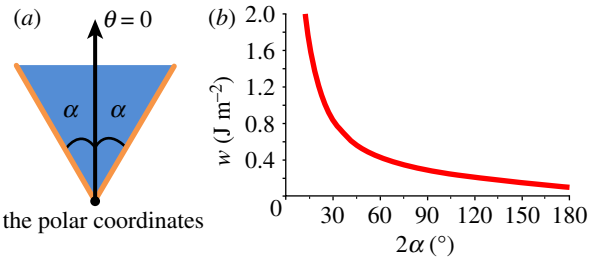

Figure 2. (*a*) The interior corner in polar coordinates (r, θ). $\theta = -\alpha$, $\theta = \alpha$ is the wedge line. The region $\theta \le -\alpha$ and $\theta \ge -\alpha$ occupied by the gold and $-\alpha \le \theta \le \alpha$ occupied by water. Line $\theta = 0$ represents the bisector of the interior angle. (*b*) The relationship between the driving work per unit area w along $\theta = 0$ and the interior angle 2α. (Online version in colour.)

Table 1. The relationship between the interior angle 2α and the averaged driving work per unit area w from molecular dynamics results.

$2\alpha(^\circ)$	26.6	45	63.4	90	116.6	135
w (J m^{-2})	0.0630	0.0920	0.1095	0.1342	0.1485	0.0943

where $A_{\mathrm{Au-Water}}$ is the Hamaker constant between the gold substrate and the water (Hamaker 1937). $A_{\mathrm{Au-Water}} = 4\pi^2 \varepsilon_{\mathrm{Au-Water}} \sigma^6_{\mathrm{Au-Water}} \rho_{\mathrm{Au}} \rho_{\mathrm{Water}} = 4.0698 \times 10^{-19}$ J, where $\varepsilon_{\mathrm{Au-Water}} = 5.2604\,\mathrm{kJ\,mol^{-1}}$ and $\sigma_{\mathrm{Au-Water}} = 0.2902$ nm are from the LJ potential, ρ is the number density ($\rho_{\mathrm{Au}} = 5.9058 \times 10^{28}\,\mathrm{m^{-3}}$ and $\rho_{\mathrm{Water}} = 3.3456 \times 10^{28}\,\mathrm{m^{-3}}$). There exists a singularity of $P \sim r^{-3}$ when r approaches 0. However, this singularity in disjoining pressure is artificial, because it does not take account of the discontinuous nature of the corner and short-range force at the contact line (Yi & Wong 2007). The PC could import atomic details to eliminate this singularity in the disjoining pressure. Considering a special case along the angular bisector, $\theta = 0$, the work performed by the disjoining pressure is

$$w(\alpha) = \int_{r_1 \sec\alpha}^{r_2 \sec\alpha} \frac{A_{\mathrm{Au-Water}}}{24\pi} r^{-3} \left(3\cot\frac{\alpha}{2} + \cot^3\frac{\alpha}{2}\right) \mathrm{d}r$$
$$= \frac{A_{\mathrm{Au-Water}}}{48\pi} \sin^2\alpha \left(3\cot\frac{\alpha}{2} + \cot^3\frac{\alpha}{2}\right)(r_1^{-2} - r_2^{-2}). \tag{3.3}$$

Because of the existence of the PC, r_1 could not reach 0, but equals $\sigma_{\mathrm{Au-Water}} \ll r_2$; so w is not sensitive to r_2. We adopted $r_2 = 5$ nm (the width of the interior corner). Then, the relationship between w and 2α was obtained in figure 2*b*. The theoretical derivations do not take account of the structure component of the disjoining pressure (Derjaguin & Churaev 1974). We also statistically obtained w from the MD results as shown in table 1. In our cases, both the theoretical and MD results confirmed $w \sim 10^{-1}\,\mathrm{J\,m^{-2}}$, the same order of the surface tension of water ($\gamma = 0.072\,\mathrm{J\,m^{-2}}$, at 298 K).

As shown in figure 3*a*, when a layer of water molecules covers the gold substrate, the most possible position of these water molecules locates at $d_0 = 2.575$ Å from the substrate. Then, the potential surfaces, whose position were labelled by blue lines in figure 3*b–d* at a distance of $d_0 = 2.575$ Å above the

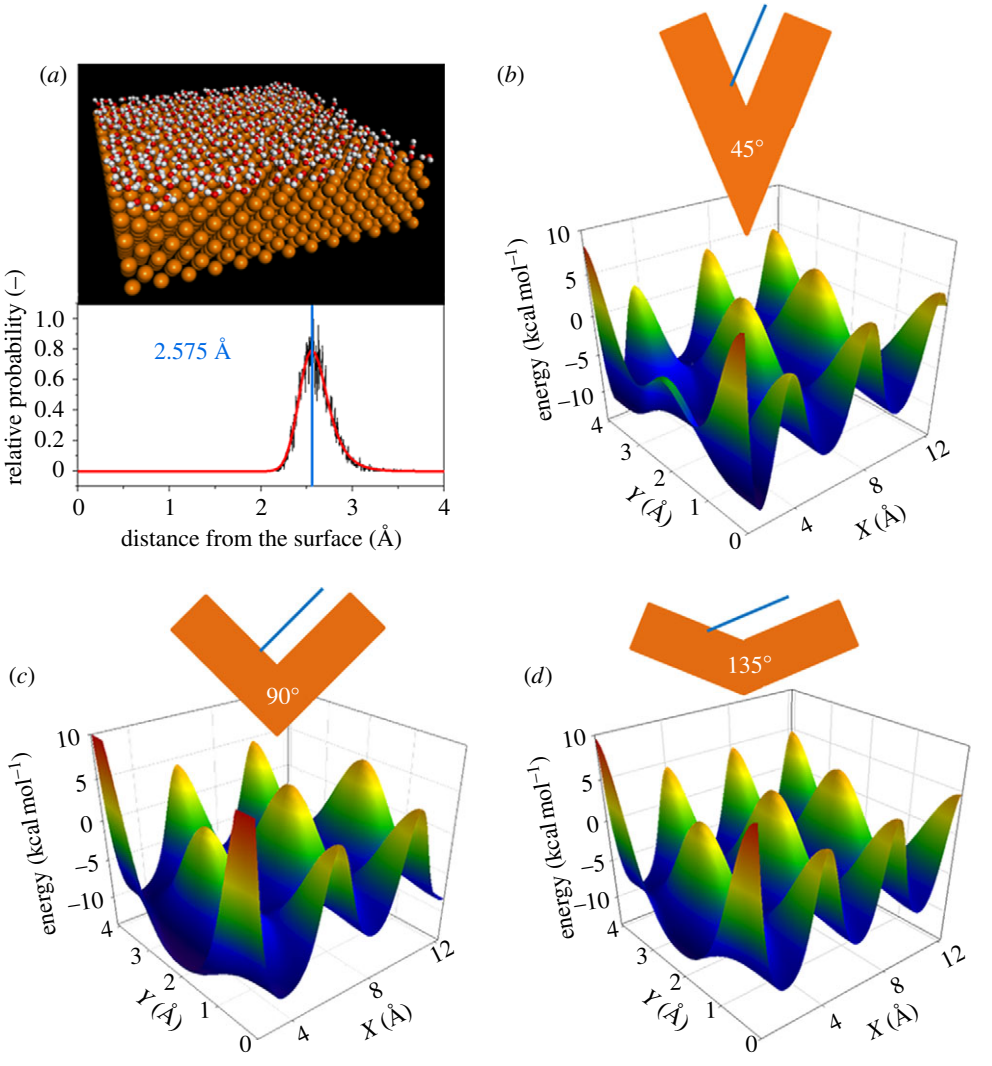

Figure 3. (*a*) A layer of water molecules on gold surface. The most possible distance d_0 of water from the surface is 2.575 Å. (*b*) For $2\alpha = 45°$, (*c*) $2\alpha = 90°$ and (*d*) $2\alpha = 135°$, the potential surface at a distance of $d_0 = 2.575$ Å from the surface. The blue line label the position of the potential surface and the direction of X coordinate. Y coordinate is the direction along the interior corner, as shown in figure 1*a*. (Online version in colour.)

substrate with different 2α ($= 45°$, $90°$ and $135°$), were scanned to obtain H as shown in figure 3*b–d*. The colour represents the height of the potential energy: the red colour represents high energy, whereas the blue colour represents low energy. Because of the crystal lattice of the gold surface, the potential surface is periodically repeated along Y direction. As the PC and PF propagated along the interior corner (Y direction), we made a projection of the potential surface on X-energy plane and obtained as shown in figure 4. The colour corresponds to that in figure 3. For the region away from the interior corner, where the PF

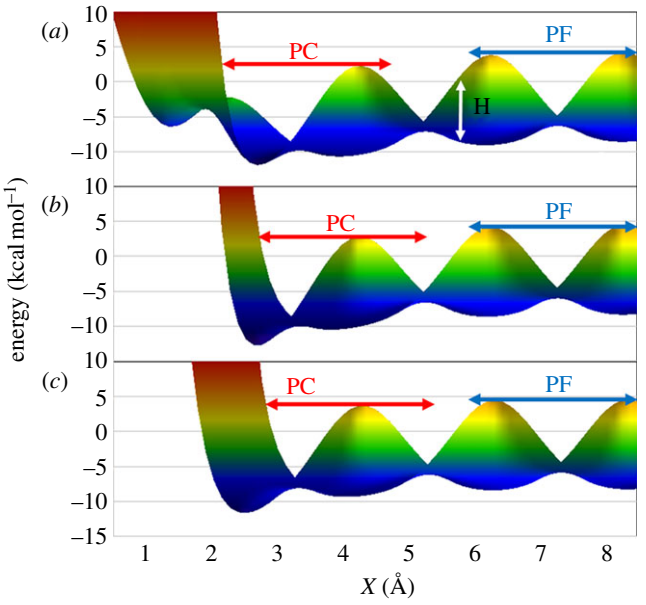

Figure 4. (*a*) For $2\alpha = 45°$, (*b*) $2\alpha = 90°$ and (*c*) $2\alpha = 135°$, the X-energy projection of the potential surface. The red and blue lines on 2.75 Å in length represent the regions where the precursor chain and the precursor film, respectively, are located. (Online version in colour.)

(the blue line in figure 4) is located, the potential surface is periodic owing to the face-centred cubic lattice of the gold [100] surface. The PC propagated on the interior corner region, whose potential surface is lower and smoother. The widths of these regions were chosen to be 2.75 Å (the diameter of a water molecule). Because water molecules were confined in the interior corner, the total vdW interactions between the two wedge surfaces reduce the potential energy at the interior corner. Hence, the adhesion energy of the PC is higher than that of the PF, which means the PC is more stable than the PF and hard to diffuse out of the corner. The confinement effect at the interior corner quickly decays in a distance of about a water molecule; so only one single-file water molecule PC was observed. The generation and stable existence of the PC could therefore be comprehended. With the increase of 2α, the energy difference between the PC and PF regions gradually vanishes. We estimated the average of the height of the potential wells in the PC and PF regions, respectively. Furthermore, we calculated the averaged velocity using equation (3.1) and produced table 2. In accord with the observation in MD simulations, v_{PC} is $0.1309\,\mathrm{ms}^{-1}$ in the case of $2\alpha = 45°$, while v_{PF} is $0.0216\,\mathrm{ms}^{-1}$. With the increase of 2α, v_{PC} decreases. In the case of $2\alpha = 135°$, $v_{PC} = 0.0297\,\mathrm{ms}^{-1}$ is nearly the same as v_{PF}, which makes PC invisible in MD simulations. For $w \ll 2nk_BT$, equation (3.1) could be written as $v \approx w/\zeta$, where $\zeta = k_BT/K_0\lambda^3 = (h/\lambda^3)\exp(H/k_BT)$ represents a friction coefficient, in Pa s units. Although $w \approx 2nk_BT \sim 0.1\,\mathrm{J\,m}^{-2}$ in our cases, we calculated the order of magnitude of ζ to understand the channel of the energy dissipation in these systems. $\zeta_{PC} \sim 1\,\mathrm{Pa\,s}$ increases with the increase of 2α, while $\zeta_{PF} \sim 10\,\mathrm{Pa\,s}$. The PC possesses less friction and dissipates less energy compared with the PF; so

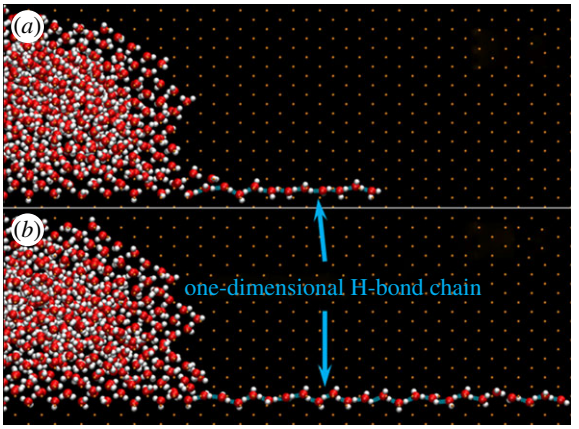

Figure 5. Side view of two transient moments (*a*) t_1; (*b*) t_2, when the PC advanced. The blue lines between water molecules represent the hydrogen bonds. (Online version in colour.)

Table 2. The average height H of the potential well, the averaged velocity v and the dynamic friction coefficient ζ in the precursor chain and the precursor film region.

	the precursor chain region			the precursor film region
2α (°)	45	90	135	
H (10^{-20}J)	4.8462	5.3820	5.4806	5.7206
v (ms^{-1})	0.1309	0.0856	0.0297	0.0216
ζ (Pa s)	1.1766	4.2899	5.4429	9.7157

the PC advances faster than the PF. In reality, the friction area $A(t)$ varied complicatedly with the time t. Because $A(t) \sim 1\,\mathrm{nm}^2$, we estimated $A(t)$ to be $1\,\mathrm{nm}^2$ in the earlier-mentioned calculations.

From the earlier-mentioned discussions about w, H, ζ and v, we can find that the low energy and low friction at the interior corner leads to the formation, stable existence and fast propagation of the PC. Next, we show the atomic details of how the PC advances diffusively. As shown in figure 5, there were H-bonds between every two adjacent water molecules in the PC, which transferred the disjoining pressure to drive water molecules along the corner. The sequence of the water molecules in the PC did not change during the whole process. To quantify our observation, we evaluated the transport properties by computing the self-diffusion coefficient D of water molecules in PC. As the PC was a single-file water-molecule chain, we considered only water diffusion in the z direction. The diffusion coefficient D is related to the slope of the mean-squared displacement by the Einstein relation:

$$D = \frac{1}{2} \lim_{t \to \infty} \left[\frac{\langle |\vec{r}(t) - \vec{r}(0)|^2 \rangle}{\Delta t} \right],$$

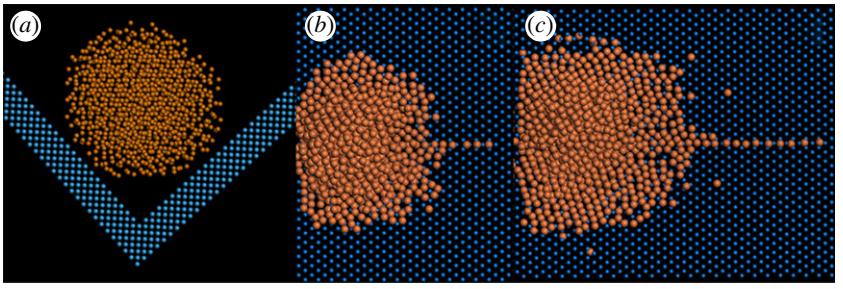

Figure 6. (*a*) Cross section of the system to form a gold metallic monatomic chain (MAC) in a tungsten interior corner. The orange and blue balls represent gold and tungsten atoms, respectively. (*b*,*c*) Top view of transient moments of formation a gold MAC. (Online version in colour.)

where $|\vec{r}(t) - \vec{r}(0)|$ is the distance travelled by molecule i over some time interval of length Δt, in which the effect of any drift in the centre-of-mass is subtracted out before the displacement of each molecule was calculated. The squared magnitude of this value was averaged over many such time intervals. The averaged $D = (0.117 \pm 0.002) \times 10^{-5}\,\mathrm{cm^2\,s^{-1}}$ of the PC is one order of magnitude less than $D = 2.246 \times 10^{-5}\,\mathrm{cm^2\,s^{-1}}$ of bulk water and $D = 1.132 \times 10^{-5}\,\mathrm{cm^2\,s^{-1}}$ of the PF (Yuan & Zhao 2010), which indicates that the PC actually acted like ice. From the atomic details, we found that (i) the disjoining pressure, transferred by one-dimensional H-bond chain, drove the PC to propagate; (ii) the PC acted like ice and slipped along the interior corner.

The PC has indeed many similar aspects as the water chain confined in nanotubes (Hummer *et al.* 2001; Won & Aluru 2008). Possessing low and smooth surface barriers (Falk *et al.* 2010), they both advance fast and are like ice (Yuan & Zhao 2009). The unique H-bonds drive them to propagate. But the differences are obvious: (i) concerning boundary condition, the PC is only confined in part, while the water chain is completely confined in the nanotube, (ii) concerning driving force, the disjoining pressure drives the PC to advance, while an external pressure is necessary in the nanotube, and (iii) concerning geometric configuration, the PC depends on the shape of the interior corner and is straight in our case, while the water chain in the nanotube has a helical structure (Yuan & Zhao 2009).

To show the possible applications of the PC, we use a melting metallic droplet to form a MAC. MAC shows great potential for nanoscale electronics (Ohnishi *et al.* 1998; Tang *et al.* 2010) for its ultimate one-dimensional structure with unique physical properties, but is nowadays limited by its short life time and short length (Yanson & Bollinger 1998; Sun *et al.* 2004). A possible solution to form a stable and long MAC might be the PC. At a constant temperature of 2500 K, a melting gold droplet was placed on a tungsten interior corner, as shown in figure 6*a*. The melting point of tungsten (3683 K) is much higher than that of gold (1337 K). Under the disjoining pressure, the gold molecules automatically formed a MAC along the tungsten interior corner. Then, a quick cooling was imposed. Using the unique transport properties of the PC, a stable and relative long gold MAC formed in figure 6*b*,*c*.

4. Conclusions

In conclusion, we performed MD simulations and MKT to explore the atomic details and transport properties of the PC in the hydrophilic interior corner with varying interior angles for the first time. A wetting transition of the PC in the interior corner was governed by the interior angle. The advance of the PC was one order of magnitude faster than the PF. Because of the confine effect in the interior corner, the potential surface was lower and smoother, making the PC propagate faster and more stably, while dissipating less energy than the PF. The self-diffusion coefficient confirmed that the PC is like ice. The one-dimensional H-bond chain made the transport properties of the PC unique. The PC could eliminate the singularity at the interior corner. Also, the formation of a gold MAC in a tungsten interior corner was simulated as an example to show the importance and applications of the PC. It is expected that our findings will help in understanding the topology-dominated dynamic wetting, expanding 'Taylor conjecture' to, and developing new applications at, nanoscale.

This work was jointly supported by the National Natural Science Foundation of China (NSFC, grant nos. 60936001, 11072244 and 11021262), the National Basic Research Programme of China (973 Programme, grant no. 2007CB310500).

References

Berendsen, H. J. C., Grigera, J. R. & Straatsma, T. P. 1987 The missing term in effective pair potentials. *J. Phys. Chem.* **91**, 6269–6271. (doi:10.1021/j100308a038)

Bonn, D., Eggers, J., Indekeu, J., Meunier, J. & Rolley, E. 2009 Wetting and spreading. *Rev. Mod. Phys.* **81**, 739–805. (doi:10.1103/RevModPhys.81.739)

Chen, Y., Weislogel, M. M. & Nardin, C. L. 2006 Capillary-driven flows along rounded interior corners. *J. Fluid Mech.* **566**, 235–271. (doi:10.1017/S0022112006001996)

Chibbaro, S., Biferale, L., Diotallevi, F., Succi, S., Binder, K., Dimitrov, D., Milchev, A., Girardo, S. & Pisignano, D. 2008 Evidence of thin-film precursors formation in hydrokinetic and atomistic simulations of nano-channel capillary filling. *Europhys. Lett.* **84**, 44003. (doi:10.1209/0295-5075/84/44003)

Concus, P. & Finn, R. 1969 On the behavior of a capillary surface in a wedge. *Proc. Natl Acad. Sci. USA* **63**, 292–299. (doi:10.1073/pnas.63.2.292)

De Gennes, P. G. 1985 Wetting: statics and dynamics. *Rev. Mod. Phys.* **57**, 827–863. (doi:10.1103/RevModPhys.57.827)

Derjaguin, B. V. & Churaev, N. V. 1974 Structural component of disjoining pressure. *J. Colloid Interface Sci.* **49**, 249–255. (doi:10.1016/0021-9797(74)90358-0)

Derjaguin, B. V., Churaev, N. V. & Muller, V. M. 1987 *Surface forces.* New York, NY: Plenum.

Falk, K., Sedlmeier, F., Joly, L., Netz, R. R. & Bocquet, L. 2010 Molecular origin of fast water transport in carbon nanotube membranes: superlubricity versus curvature dependent friction. *Nano Lett.* **10**, 4067–4073. (doi:10.1021/nl1021046)

Gladstone, S., Laidler, K. & Eyring, H. 1941 *The theory of rate processes.* New York, NY: McGraw-Hill.

Gleiche, M., Chi, L. & Fuchs, H. 2000 Nanoscopic channel lattices with controlled anisotropic wetting. *Nature* **403**, 173–175. (doi:10.1038/35003149)

González, M. A. & Abascal, J. L. F. 2010 The shear viscosity of rigid water models. *J. Chem. Phys.* **132**, 096101. (doi:10.1063/1.3330544)

Hamaker, H. 1937 The London–van der Waals attraction between spherical particles. *Physica* **4**, 1058–1072. (doi:10.1016/S0031-8914(37)80203-7)

Herminghaus, S., Brinkmann, M. & Seemann, R. 2008 Wetting and dewetting of complex surface geometries. *Annu. Rev. Mater. Res.* **38**, 101–121. (doi:10.1146/annurev.matsci.38.060407.130335)

Huh, C. & Scriven, L. 1971 Hydrodynamic model of steady movement of a solid/liquid/fluid contact line. *J. Colloid Interface Sci.* **35**, 85–101. (doi:10.1016/0021-9797(71)90188-3)

Hummer, G., Rasaiah, J. C. & Noworyta, J. P. 2001 Water conduction through the hydrophobic channel of a carbon nanotube. *Nature* **414**, 188–190. (doi:10.1038/35102535)

Kavehpour, H. P., Ovryn, B. & McKinley, G. H. 2003 Microscopic and macroscopic structure of the precursor layer in spreading viscous drops. *Phys. Rev. Lett.* **91**, 196104. (doi:10.1103/PhysRevLett.91.196104)

Khare, K., Herminghaus, S., Baret, J.-C., Law, B. M., Brinkmann, M. & Seemann, R. 2007 Switching liquid morphologies on linear grooves. *Langmuir* **23**, 12997–13006. (doi:10.1021/la701899u)

Kwon, Y., Patankar, N., Choi, J. & Lee, J. 2009 Design of surface hierarchy for extreme hydrophobicity. *Langmuir* **25**, 6129–6136. (doi:10.1021/la803249t)

Mark, P. & Nilsson, L. 2001 Structure and dynamics of the TIP3P, SPC and SPC/E water models at 298 K. *J. Phys. Chem. A* **105**, 9954–9960. (doi:10.1063/1.1329346)

Ohnishi, H., Kondo, Y. & Takayanagi, K. 1998 Quantized conductance through individual rows of suspended gold atoms. *Nature* **395**, 780–783. (doi:10.1038/27399)

Patra, N., Wang, B. & Kraìl, P. 2009 Nanodroplet activated and guided folding of graphene nanostructures. *Nano Lett.* **9**, 3766–3771. (doi:10.1021/nl9019616)

Philip, J. 1977 Adsorption and geometry: the boundary layer approximation. *J. Chem. Phys.* **67**, 1732–1741. (doi:10.1063/1.435056)

Plimpton, S. 1995 Fast parallel algorithms for short-range molecular-dynamics. *J. Comput. Phys.* **117**, 1–19. (doi:10.1006/jcph.1995.1039)

Rascón, C. & Parry, A. 2000 Geometry-dominated fluid adsorption on sculpted solid substrates. *Nature* **407**, 986–989. (doi:10.1038/35039590)

Seemann, R., Brinkmann, M., Kramer, E., Lange, F. & Lipowsky, R. 2005 Wetting morphologies at microstructured surfaces. *Proc. Natl Acad. Sci. USA* **102**, 1848–1852. (doi:10.1073/pnas.0407721102)

Spernjak, D., Prasad, A. & Advani, S. 2007 Experimental investigation of liquid water formation and transport in a transparent single-serpentine PEM fuel cell. *J. Power Sources* **170**, 334–344. (doi:10.1016/j.jpowsour.2007.04.020)

Sun, C. Q., Bai, H. L., Li, S., Tay, B., Li, C., Chen, T. & Jiang, E. 2004 Length, strength, extensibility, and thermal stability of a Au–Au bond in the gold monatomic chain. *J. Phys. Chem. B* **108**, 2162–2167. (doi:10.1021/jp035815j)

Tang, D.-M. *et al.* 2010 Carbon nanotube-clamped metal atomic chain. *Proc. Natl Acad. Sci. USA* **107**, 9055–9059. (doi:10.1073/pnas.0914970107)

Taylor, B. 1712 Concerning the ascent of water between two glass planes. *Phil. Trans.* **27**, 538. (doi:10.1098/rstl.1710.0070)

Vega, C. & De Miguel, E. 2007 Surface tension of the most popular models of water by using the test-area simulation method. *J. Chem. Phys.* **126**, 154707. (doi:10.1063/1.2715577)

Wang, C., Lu, H., Wang, Z., Xiu, P., Zhou, B., Zuo, G., Wan, R., Hu, J. & Fang, H. P. 2009 Stable liquid water droplet on a water monolayer formed at room temperature on ionic model substrates. *Phys. Rev. Lett.* **103**, 137801. (doi:10.1103/PhysRevLett.103.137801)

Wang, C.-X., Xu, S.-H., Sun, Z.-W. & Hu, W.R. 2010 A study of the influence of initial liquid volume on the capillary flow in an interior corner under microgravity. *Int. J. Heat Mass Transfer* **53**, 1801–1807. (doi:10.1016/j.ijheatmasstransfer.2010.01.009)

Webb, E. B., Grest, G. S. & Heine, D. R. 2003 Precursor film controlled wetting of Pb on Cu. *Phys. Rev. Lett.* **91**, 236102. (doi:10.1103/PhysRevLett.91.236102)

Weislogel, M. M. & Lichter, S. 1996 A spreading drop in an interior corner: theory and experiment. *Microgravity Sci. Technol.* **9**, 175–184.

Weislogel, M. M. & Lichter, S. 1998 Capillary flow in an interior corner. *J. Fluid Mech.* **373**, 349–378. (doi:10.1017/S0022112098002535)

Whitby, M. & Quirke, N. 2007 Fluid flow in carbon nanotubes and nanopipes. *Nat. Nanotechnol.* **2**, 87–94. (doi:10.1038/nnano.2006.175)

Won, C. Y. & Aluru, N. R. 2008 Water phase transition induced by a Stone–Wales defect in a boron nitride nanotube. *J. Am. Chem. Soc.* **130**, 13649–13652. (doi:10.1021/Ja803245d)

Yanson, A. & Bollinger, R. 1998 Formation and manipulation of a metallic wire of single gold atoms. *Nature* **395**, 783–785. (doi:10.1038/27405)

Yi, T. & Wong, H. 2007 Theory of slope-dependent disjoining pressure with application to Lennard–Jones liquid films. *J. Colloid Interface Sci.* **313**, 579–591. (doi:10.1016/j.jcis.2007.05.015)

Young, T. 1805 An essay on the cohesion of fluids. *Phil. Trans. R. Soc. Lond.* **95**, 65–87. (doi:10.1098/rstl.1805.0005)

Yuan, Q. Z. & Zhao, Y. P. 2009 Transport properties and induced voltage in the structure of water-filled single-walled boron-nitrogen nanotubes. *Biomicrofluidics* **3**, 022411. (doi:10.1063/1.3158618)

Yuan, Q. Z. & Zhao, Y. P. 2010 Precursor film in dynamic wetting, electrowetting and electro-elasto-capillarity. *Phys. Rev. Lett.* **104**, 246101. (doi:10.1103/PhysRevLett.104.246101)